Title

Structure of Copper–Cobalt Surface Alloys in Equilibrium with Carbon Monoxide Gas

Permalink

https://escholarship.org/uc/item/0q34s4r2

Journal

Journal of the American Chemical Society, 140(21)

ISSN

0002-7863

Authors

Eren, Baran
Torres, Daniel
Karslıoğlu, Osman
et al.

Publication Date

2018-05-30

DOI

10.1021/jacs.7b13621

Peer reviewed

The Structure of Copper-Cobalt Surface Alloys in Equilibrium with Carbon Monoxide Gas

Baran Eren[1,*], Daniel Torres[2], Osman Karslıoğlu[3], Zongyuan Liu[4], Cheng Hao Wu[1], Dario Stacchiola[4,**], Hendrik Bluhm[3,5], Gabor A. Somorjai[1,6], Miquel Salmeron[1,7,***]

[1]*Materials and *[3]*Chemical Sciences Divisions, Lawrence Berkeley National Laboratory, 1 Cyclotron Road, Berkeley, California 94720, United States,*

[2]*Department of Science, BMCC-The City University of New York, New York 10007, United States,*

[4]*Chemistry Department, Brookhaven National Laboratory, Upton, New York 11973, United States,*

[5]*Advanced Light Source, Lawrence Berkeley National Laboratory, 1 Cyclotron Road, Berkeley, California 94720, United States,*

[6]*Chemistry and *[7]*Materials Science and Engineering Departments, University of California, Berkeley, United States*

[*] Current address: *Department of Chemical and Biological Physics, Weizmann Institute of Science, 234 Herzl Street, 7610001 Rehovot, Israel*

[**] Current address: *Center for Functional Nanomaterials, Brookhaven National Laboratory, Upton, New York 11973, United States*

[***] E-mail: mbsalmeron@lbl.gov, Phone: +1-510-486-6704

Abstract

We studied the structure of the copper-cobalt (CuCo) surface alloy, formed by Co deposition on Cu(110), in dynamic equilibrium with CO. Using scanning tunneling microscopy (STM), we found that in vacuum at room temperature and at low Co coverage, clusters of a few Co atoms

substituting Cu atoms form at the surface. At CO pressures in the Torr range, we found that up to 2.5 CO molecules can bind on a single Co atom, in carbonyl-like configurations. Based on high-resolution STM images, together with density function theory calculations, we determined the most stable CuCo cluster structures formed with bound CO. Such carbonyl-like formation manifests in shifts in the binding energy of the Co core-level peaks in x-ray photoelectron spectra, as well as shifts in the vibrational modes of adsorbed CO in infrared reflection absorption spectra. The multiple CO adsorption on a Co site weakens the Co-CO bond and thus reduces the C-O bond scission probability. Our results may explain the different product distribution, including higher selectivity towards alcohol formation, when bimetallic CuCo catalysts are used compared to pure Co.

1. INTRODUCTION

Our present fundamental understanding of catalyst surfaces has benefited from the use of model single crystals and surface sensitive techniques that work under conditions of ultra-high vacuum (UHV), often performed at cryogenic temperatures.[1,2] To approach conditions closer to those in practical catalysis research the field has evolved into new directions: One is the use of complex surfaces, such as oxide supports and bimetallic catalysts; another is to operate under gaseous or liquid environments. The latter has been made possible by the development of new microscopy tools such as high pressure scanning tunneling microscopy (HPSTM),[3-6] environmental transmission electron microscopy, x-ray based spectroscopies like ambient pressure x-ray photoelectron spectroscopy (APXPS),[7-9] x-ray absorption spectroscopy (XAS), and optical techniques such as infrared reflection absorption spectroscopy (IRRAS).[10,11]

Using combinations of such characterization techniques it was found that even the most compact and stable surfaces could go through substantial structural and chemical changes when in equilibrium with reactant gases. For instance, using HPSTM and APXPS, it was observed that the (111), (100), and (110) faces of Cu break up into nanoclusters at room temperature (RT ~ 298 K) in the presence of CO gas at pressures above 0.1 Torr.[12-14] Density functional theory (DFT), on the other hand, has been a key computational tool for understanding the atomic structures observed by STM and for understanding the energetics of densely covered surfaces at RT and above.[12,13]

Many bimetallic or multi-component alloys have shown very different, and sometimes promising, catalytic activity and selectivity compared to elemental metal catalysts. The tunability of the catalyst composition allows us to further optimize the selectivity towards high value products.[15,16] For example, copper-cobalt (CuCo) alloys are reported to enhance the selectivity towards oxygenated products in Fischer-Tropsch synthesis from syngas (CO + H_2),[17-23] while pure Co produces mostly olefins and paraffins.[24] Bimetallic CuCo systems in the form of single crystals or core-shell nanoparticles have been studied in the past, and the effect of reactant gases in modifying their structure has been demonstrated to a certain extent.[25-28] However, their atomic structure and chemical state in the presence of gases in the Torr pressure range remains largely unexplored. For that reason we used a model Cu(110) single crystal onto which we evaporated Co to produce a well-defined surface alloy. Here, using HPSTM, APXPS, IRRAS, and DFT we determined the atomic and chemical structure of the bimetallic CuCo surface in the presence of CO in the Torr pressure range.

2. EXPERIMENTAL

The experiments were carried in three different experimental systems, each with a UHV preparation chamber containing tools such as Ar ion sputtering for cleaning, metal evaporators, quartz crystal microbalance (QCM) for thickness monitoring, mass spectrometer, and Auger electron spectrometer (AES). The preparation chamber connects through a gate valve to an analysis/reaction environmental chamber containing either microscopy or a spectroscopy technique. In the first system, the reaction chamber contained a custom-made STM instrument operating both in UHV and in gases at pressures in the Torr to atmospheric range. The second system was devoted to APXPS, at beam line 11.0.2 of the Advanced Light Source, the Berkeley Synchrotron Facility. The third system, located at the Brookhaven National Laboratory was equipped with IRRAS to determine the vibrational structure of adsorbed CO. The same Cu(110) single crystal was used in each system. For each experiment, the CO gas was passed through a Ni-carbonyl trap at 513 K prior to introduction to the chamber, where the initial base pressure was in the low 10^{-10} Torr range. In the HPSTM and IRRAS chambers, AES was used to monitor the chemical composition before the experiments and to monitor the Co content of the surface, and again after the experiment to make sure that no Ni contamination had built up on the surface.

The pressure, in the Torr range, was measured with a MKS 722A Baratron capacitance pressure gauge. All measurements were performed at RT unless otherwise indicated.

HPSTM imaging was performed using Pt-Ir tips with the bias voltage applied to the sample.[4] For APXPS experiments photon energies of 1150 eV for Cu 2p, 1000 eV for Co 2p, 490 eV for C 1s, and 735 eV for O 1s were used to produce photoelectrons with kinetic energies around 200 eV in all cases. The peak energies were referred to the Fermi level, measured in the same spectrum at the corresponding photon energy. The IRRA spectra were collected with a resolution of 4 cm^{-1} at grazing incidence with a commercial Fourier transform infrared (FTIR) spectrometer (Bruker, IFS 66v/S).[29]

The CuCo surface alloy was prepared as follows: first the Cu(110) surface was cleaned by several cycles of Ar ion sputtering (1×10^{-5} Torr, 1 kV, 15 min) and annealing to 823 K for 10 min. Following the recipe in Ref.[30], prior to Co deposition a chemisorbed oxygen layer was created on Cu(110) by exposure to 10 Langmuir of O_2 at 600 K, followed by 5 min annealing at the same temperature. The role of oxygen is to lower the surface energy for the subsequent growth of Co layers, since the oxygen always resides on the top layer during growth. It also prevents contamination from the background gases. During Co deposition, a CuCo surface alloy is formed as Co displaces Cu atoms while alternating metal-oxygen-metal chains of the (2×1) structure are maintained. Consequently, the surface splits into two levels, the second level made of the aggregated 2D Cu islands with additional Co (Figure S6). The capping oxygen could later be removed by exposure to 0.1 Torr CO at RT. Except where indicated, in most of the experiments reported here the surface population of Co was kept at approximately 20% of the surface atoms.

3. THEORY

To support the interpretation of the CuCo and adsorbed CO structures we performed first-principles calculations within the framework of DFT, using the grid-based projector-augmented wave code GPAW,[31] with a grid spacing of 0.18 Å. The projected augmented wave (PAW) method was employed to describe the effect of the inner cores of the atoms on the valence electrons.[32,33] The exchange-correlation energy and potential are described using the generalized gradient approach for the exchange-correlation functional within the Perdew-Wang (PW91) implementation.[34,35] The metal substrate was modeled by a (4×2) periodic slab consisting of four

(110) atomic planes. An experimental lattice parameter of 3.61 Å was employed for the Cu matrix in all calculations, while the atoms in three outermost atomic layers were allowed to relax. In all the calculations periodic boundary conditions in the X and Y directions were employed. Equilibrium nuclear positions were determined by minimization of the acting force in a quasi-Newton scheme until the maximum force was smaller than 0.01 eV.Å^{-1}. The Brillouin zone was sampled using a 2×2×1 Monkhorst-Pack grid. The alloy composition was fixed at 6.25% Co, equivalent to 0.25 monolayers (ML) of surface Co atoms.

4. RESULTS and DISCUSSION

4.1. STM and XPS characterization

Figure 1a shows an STM image of the initial clean surface in UHV, showing the expected atomic spacing of ~2.6 Å and ~3.6 Å in the [1-10] and [001] crystallographic directions. A Cu(110)-(2×1)-O surface structure was obtained after oxygen adsorption, which consists of Cu-O chains along the [001] direction (Figure 1b). Figure 1c shows an image after deposition of 0.2 ML of Co on this surface, where the Co atoms are randomly positioned substituting Cu atoms in the metal-O chains. The expanded area marked with a box, in derivative form, reveals M-O-M (M = Cu or Co) chains similar to those in the initial Cu(110)-(2×1)-O surface, with varying contrast along the chains due to the higher contrast (i.e., 0.1-0.2 Å brighter in the image) of the Co atoms. The islands on top of the terraces contain about 20% of all surface atoms, and are composed of Co atoms, and Cu atoms displaced from the surface. At higher Co coverage other two- and three-dimensional Co and CuCo clusters are produced (not shown here).

The removal of O from this surface by reaction with CO at RT was followed by APXPS as a function of the CO gas pressure, from 10^{-10} Torr to 0.5 Torr. As shown in Figure 2, no appreciable change in composition is apparent until 0.01 Torr, after which a rapid removal of chemisorbed O, from 0.5 ML to ~0.05 ML occurred (red dots in Figure 2c). This was accompanied by an increase in CO coverage, from 0 to 0.5 ML (black dots in Figure 2c). For comparison the coverage of CO on the clean Cu(110) is also shown (cross symbols in Figure 2c). After evacuation of the CO gas phase, the coverage of chemisorbed CO remained unchanged, although a small increase in atomic O occurred, likely due background contamination.
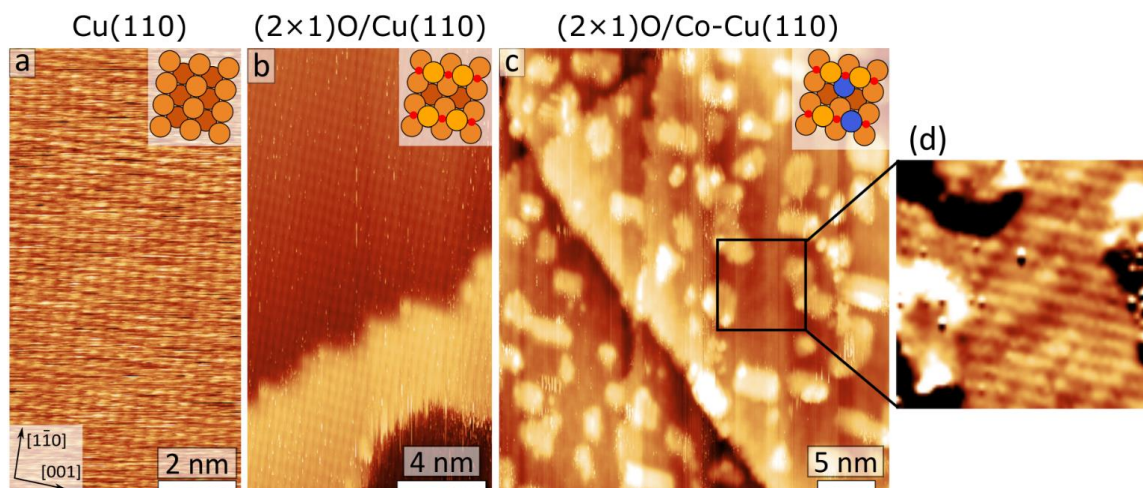
Fig. 1 STM images acquired at each step of the sample preparation process: (a) (1×1) Cu(110) surface. (b) Cu(110)-(2×1)-O surface. (c) After 0.2 ML of Co deposition. Co atoms and Cu atoms displaced from the initial surface form 2D islands. The Co atoms, which have a slightly higher apparent STM contrast than Cu atoms produce a varying contrast along the M-O chains. (d) Expanded derivate image of area marked by the box. Derivative imaging enhances the contrast variations along the M-O chains. In the ball model insets Cu, Co, and O atoms are shown in orange, blue, and red, respectively.
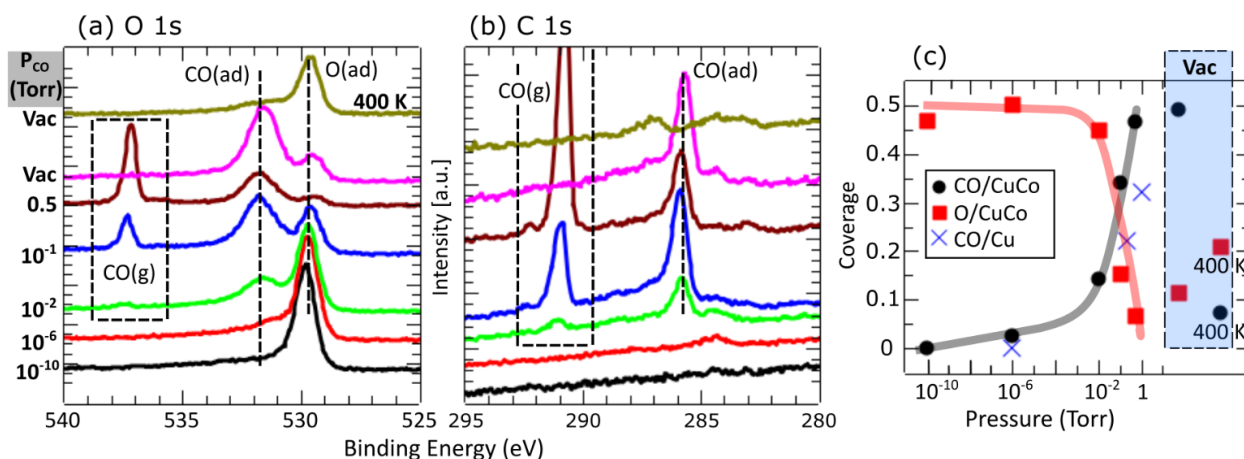
Fig. 2 (a) O 1s, and (b) C 1s, regions of the XPS spectrum of the CuCo surface alloy (20% Co-80% Cu) under various CO pressures. The attenuated peak intensities at higher gas pressure are due to increased scattering of photoelectrons by gas phase molecules. The surface is initially covered with oxygen, which produces the peak at 529.9 eV. The C and O peaks from CO_{ads} appear at 531.9 eV and 285.7 eV, similar to those of CO_{ads} on Co (Figure S1). The gas phase CO peaks are shown enclosed by a dashed box, their exact position depanding on the surface work function. The graphs in (c) show the coverage of CO (●) and O (■) vs CO presssure. The CO reacts and removes O from the surface at appreciable rates above 0.01 Torr. The CO coverage on pure Cu(110) in equilibirum with the CO pressure is shown for reference (×). The box on the right shows the coverage after evacuation (Vac), and after heating to 400 K. Coverage of different species as a function of pressure in (c) was determined from the O 1s peak intensities with respect to the Cu 2p + Co 2p peak intensities measured at the same kinetic energy, and using the well-known 0.5 ML coverage of the (2×1) oxide structure as reference.

Since the XPS peaks of CO/CuCo (Figures 2a and b) are similar to those on CO/Co (Figure S1 of the Supporting Information (SI)), we conclude that the majority of the CO molecules are bound to Co, or to Cu atoms modified by binding to Co. DFT calculations and other experimental techniques discussed below show that the former case is correct. Since the Co coverage is ~0.2 ML, this implies that more than one CO molecule is bound per Co atom on average. This interesting and unexpected result is in line with a 3-decades old result of CO adsorption on Co clusters deposited on Cu(100), obtained with AES and thermal desorption spectroscopy.[36]

The changes in the chemical state of Co due to CO adsorption were followed by the shifts in binding energy (BE) of its $2p_{3/2}$ core levels and by the changing intensities of the Co^0 and Co^{2+} components, as shown in Figure 3. The intensities of the Co^0 and Co^{2+} peaks and their satellites were measured by fitting them according to the procedure suggested in Ref.[37] (examples shown by the red and blue curves for the UHV spectra). We find that initially about half of the Co appears as Co^{2+}, located on the top M-O rows, whilst the other half, corresponding to Co^0, is located in the second layer. This ratio remained unchanged under CO gas up to 0.01 Torr where it started to decrease (Figure 3b) due to reduction of the Co^{2+}. At 0.5 Torr reduction to the metallic state proceeds rapidly, and only small amounts of Co^{2+} remain (Figure 3b). The Cu atoms on the other hand are fully reduced at this pressure.[38] Particularly interesting is the shift in the Co^0 $2p_{3/2}$ BE observed in these experiments, where the Co coverage is 0.2 ML (Figure 3c black dots). At Co coverages above 0.5 ML (red dots), where Co and CoO form larger islands, no shift was observed. The shift of the Co $2p_{3/2}$ peak to a higher BE indicates an increasing donation of electrons from Co to CO, which we ascribe to binding of multiple CO molecules per Co atom, similar to the structure of Co-carbonyl species. This is only possible if Co is in the form of isolated atoms or few atom clusters where the bound CO molecules can fan out to accommodate their steric repulsion. As we show below DFT calculations indicate that the Co atoms in the second layer are pulled out to the top layer by CO chemisorption, where it forms small clusters.
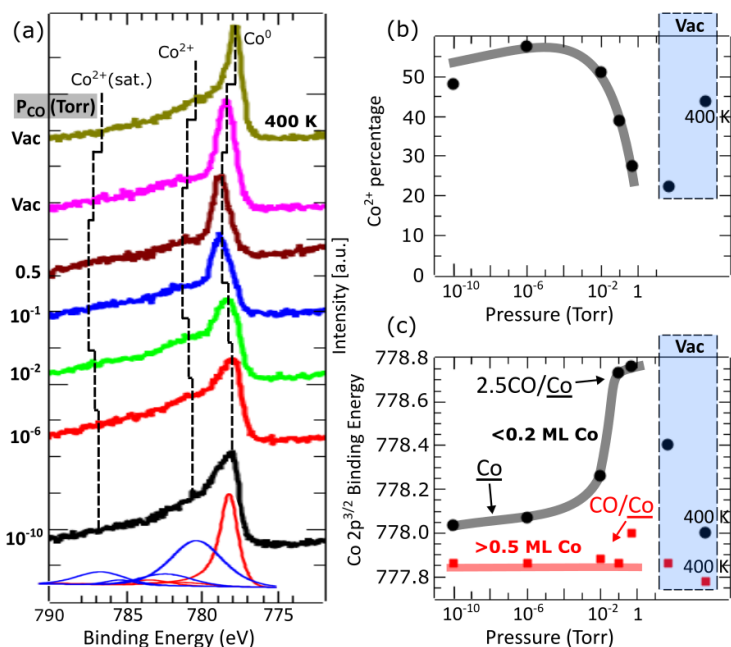
Fig. 3 (a) Co $2p_{3/2}$ XP spectra acquired at RT as a function of increasing CO pressure, from UHV (bottom black spectrum) to 0.5 Torr (brown). The two spectra at the top were collected after CO evacuation (pink) and after heating the sample to 400 K (top, dark yellow). Co $2p_{3/2}$ has satellite peaks from Co^0 and Co^{2+}, were fitted with the red (Co^0) and blue (Co^{2+}) curves, shown only for the initial spectrum in UHV (bottom). The amount of Co^{2+} decreases above 0.01 Torr (b), while CO coverage increases (c). The Co XPS peaks shift to higher binding energy (black curve in (c)), following the increasing number of CO molecules per Co atom at low Co coverage. No XPS shifts were observed when the Co coverage was >0.5 ML (red dots in (c)) due to steric contraints preventing multiple CO binding per Co atom (except possibly at island edge atoms).

In agreement with XPS, the STM images confirmed the removal of the oxide structure on the surface as the CO pressure increased (Figures S5-S6). After the (2×1) oxide structure is removed the surface is covered with 2D nanoclusters of irregular shape (Figure S7). Figure 4 shows an atomically resolved image, where the clusters appear as dimer rows at pressures above 0.5 Torr. The dimers appear as pairs of bright spots along the [110] direction separated by 3.5 Å, substantially larger than the atomic lattice spacing of 2.55 Å. We explain this by assigning the maxima to CO molecules that are adsorbed on the top sites and tilted away from each other due to steric repulsion. On the [001] direction the periodicity is 3 Å, which is less that the atomic periodicity 3.61 Å in that direction. We attribute this adsorption geometry to the formation of locally dense CO structures with more than one molecule per Co atom, as shown schematically in Figure 4c. From IRRAS (see below) we know that CO adsorbs both on top and on bridge Co sites, so that the observed STM contrast can originate from combinations of 3 CO (2 top sites, 1

8

bridge site) and 5 CO (4 top sites, 1 bridge site) molecules. According to our model in Figure 4c, CO molecules at the bridge sites have a very low STM contrast, because in mixed top and bridge or hollow CO sites, the STM contrast is dominated by that of the top sites.[12,39-40] While from STM imaging only it is not possible to prove this at present, both IR spectra and DFT calculations (shown later) indicate that CO molecules occupy both atop and bridge sites simultaneously. In fact, DFT calculations support this model by showing that isolated 2-Co-atom clusters accommodating 5 CO molecules are energetically favored.

It should also be pointed out that the surface has a considerable number steps with heights of 1 and two atoms. An alternative structure is one where CO adsorbs only on top sites in the terraces (same as in Figure 4c, but with the bridge CO molecules missing), with CO adsorption on the bridge sites occurring only at step edges. This alternative model, however, is not supported by the DFT calculations, which show that additional CO molecules adsorb on the bridge sites before two CO molecules start occupying a single CO site.
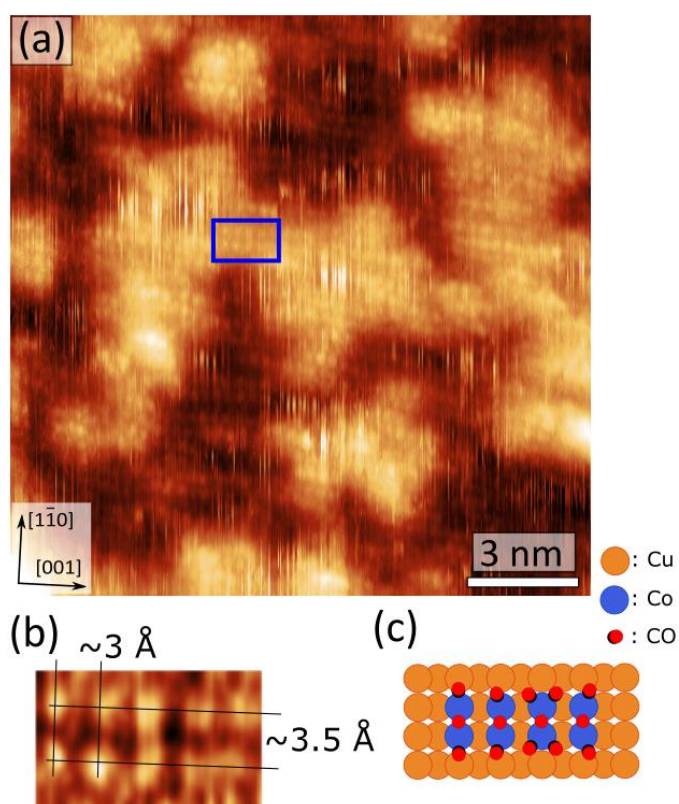

Fig. 4 (a) STM image of the CuCo surface under 3 Torr CO. The maxima are assigned to CO molecules bound to top Co sites forming dimers in short rows along the [100] direction, as indicated in the expanded area below (b). (c) is the surface structure of the suggested model. According to this model, we can estimate 1.75 CO to be on the Co sites, equivalent to 0.35 ML nominal coverage. The rest of CO (0.15 ML nominal coverage) should be on the Cu sites, which constitute 80% of the surface, hence roughly 0.19 CO per Cu site.

4.2 IRRAS studies

In addition to XPS and STM, we studied the CO adsorption after oxide removal with

IRRAS. The high structural sensitivity of the technique makes it ideal to study fine details of the adsorption of CO, thus providing a complementary identification of the adsorption sites. As suggested by Toomes and King,[41] CO adsorbed on top metallic sites has C-O stretching frequencies in the 2000-2130 cm^{-1} range, whereas on bridge sites the frequency range is 1860-2000 cm^{-1}. On clean Cu surfaces, at pressures below 1 Torr, CO adsorbs only on top sites with frequencies in the 2070-2106 cm^{-1} range.[42]

Weakening of the CO-metal bond decreases back bonding donation to the antibonding π^* orbitals thus strengthening the C-O bond and shifting the C-O stretch frequency to higher values. The CO-metal bonding strength depends also on the type of metal, e.g., Cu, Co, site coordination (top, bridge, hollow), and is expected to decrease also by repulsion between CO molecules adsorbed on a single Co site. Figure 5 shows IRRAS data of the 0.2 ML of CuCo surface in the presence of CO at various pressures. No adsorbed CO peak is visible at pressures below 10^{-2} Torr (red curve), where the surface is still oxidized (0.5 ML of O). At 0.1 Torr CO, when most of the oxide is reduced to metal, a CO peak is observed at a frequency corresponding to bridge sites at 1983 cm^{-1}. The peak shifts to higher frequencies at 0.5 Torr (peaks 4', 3', 2' and 1'), between 2000 cm^{-1} to 2100 cm^{-1}. Peak 1' matches the frequency for top Cu sites, 2' to that of multiple molecules per Co atom in small clusters or at edges, and 3' to top Co sites.[43] The shifts in CO stretch frequencies due to multiple CO binding in Co-carbonyl molecules were reported in Ref. [44,45] Carbonyl-like CO adsorption was also observed in surface science studies[46], which show that two CO molecules can adsorb to isolated Rh atoms and or on few atom clusters, with a blue shift in the CO symmetric stretch frequency compared to CO adsorbed on larger Rh islands.

The high frequency peaks disappear upon evacuation of the gas phase, leaving only the 5' peak from the bridge sites (cyan curve). A new peak (6'), observed after evacuation could be due to the CO bound to unreduced Co^{2+} residuals.[47] Although CO might not be stable at RT on Co^{2+} sites on bulk Co oxides, it may be different here where the Co^{2+} may be affected by the Cu substrate, as seen previously for CO adsorption on Cu^+ being stronger when it is linked to Ti.[48] This 6' feature is likely to be there in the presence of CO as well, but coincides with the gas phase features.
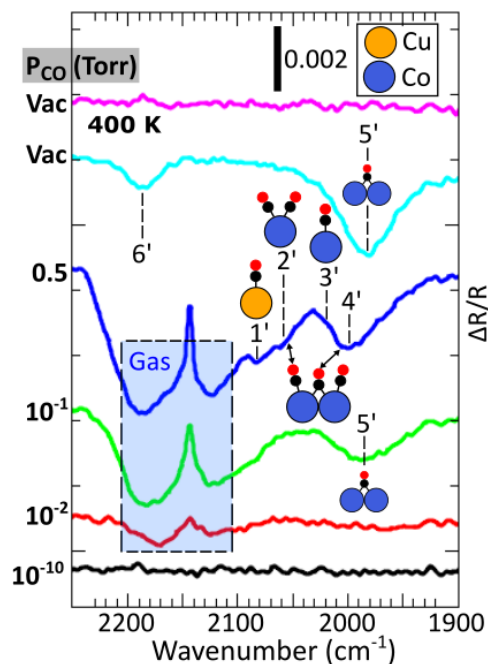
Fig. 5 IRRAS spectra of CO on the CuCo surface in the presence of CO gas at different pressures. Gas phase peaks are visible above 0.01 Torr, by the broad bands between 2100-2200 cm^{-1}. Adsorbed species are indicated with the prime symbol ('), and are explained in the main text.

The above assignments are supported by the additional spectra acquired from CO on pure Cu(110), on Cu(110)-(2×1)O and on CuCo at cryogenic temperatures, shown in the SI (Figures S3 and S4). Similarly, Figure S5 shows the spectra of CO adsorbed on 10 ML of Co.

Although the shifts in Co 2p spectra to higher binding energies and the shifts to higher wavenumbers of the CO stretching frequencies as the CO pressure increases appear at first contradictory, this is not the case. The IR blue shift suggests less back donation to *a single CO*, with the XPS shift is due to more electron donation *from Co to multiple CO molecules.* Finally, we would like to remark on the 1' peak in Figure 5 (CuCo surface at 0.5 Torr) being significantly less intense than the 1' peak in Figure S3 in SI (bare Cu(110) surface at 0.5 Torr). This might potentially be due to a similar effect observed on the deposition of Fe on Cu surfaces, i.e., CO attached to Cu atoms that are intermixed with Fe atoms with a specific surface lattice structure.[49] However, in line with our APXPS spectra and the DFT calculations shown below, we think that this is simply a steric effect of CO covering the Co sites and preventing CO from attaching to the neighboring Cu sites. In other words, the local CO coverage on the Cu sites is significantly less than local CO coverage on the Co sites.

4.3 DFT calculations

To determine the equilibrium structure of the CO/CuCo system formed on Cu(110) by deposition of 0.2 ML of Co, we calculated the surface Gibbs free energy $\Delta G(\theta,\chi)$ at fixed T-p conditions (1 Torr CO at RT, see SI).[50] Figure 6 shows a 3D plot of ΔG (in color) as a function of CO coverage (θ), and fraction of Co atoms in the top layer (χ). At zero CO coverage the calculations predict that Co atoms are preferentially located in the second layer in the Cu(110) matrix (point 1 in the diagram, top structure 1). This agrees with the surface segregation trends found in the literature,[51-53] where adsorption of CO causes Co atoms to segregate to the top layer where it bounds to CO (point 2 in the diagram, top structure 2). As the CO coverage reached approx. 0.75 ML (red area in the diagram), all Co atoms are in the top layer bound to CO molecules. The most energetically stable structure, point 4 in the diagram, has an average occupancy of 2.5 CO molecules per Co atom, as shown as the structure 4 in the top schematic.
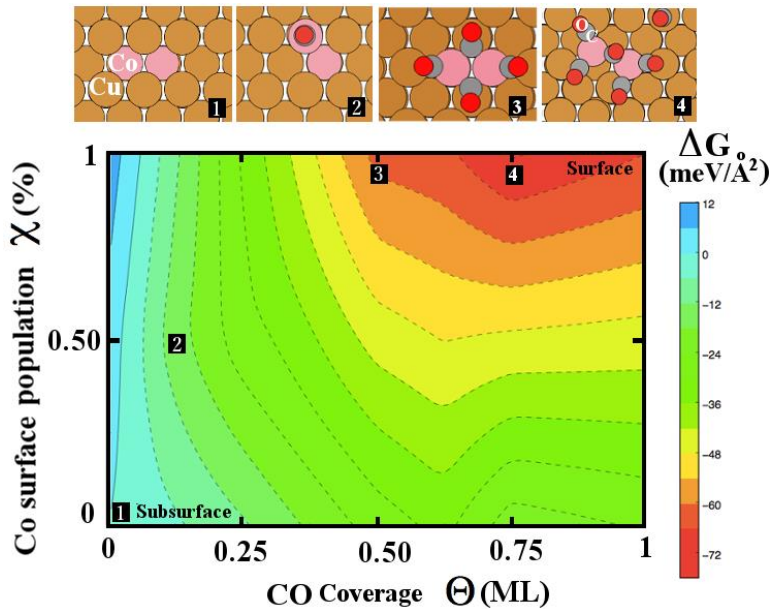

Fig. 6 Gibbs free energy ΔG in the parameter space of χ (Co surface population, Y-axis) and θ (CO coverage, X-axis), in equilibrium with 1 Torr of CO at RT. The percentage of Co atoms is fixed at 20% in the surface alloy formed on the surface of Cu(110), with the Co atoms occupying sites in the first or second layer. The color scale in the right hand side indicates the values of ΔG quantifying the stability of the different CO/CuCo phases. Selected atomic structures at points 1, 2, 3 and 4 are shown at the top,. Cu atoms are shown in ocher color and the Co atoms in pink. Structure 4 is the most stable configuration.

We next address the impact of temperature and CO pressure. In Figure 7, we display the T-p phase diagrams for a CuCo(110) surface in equilibrium with a surrounding CO gas phase environment. The most stable CuCo phase at high temperatures and low CO pressures (Figure 7;

bottom right) corresponds to the bare CuCo substrate, with the Co atoms located in the second layer. Figure 7 also shows the relevant phases in the whole range of experimentally accessible pressure conditions, 10^{-13} to 10^{3} Torr, indicating the stability of CO/CuCo phases with 0.50 and 0.75 ML CO coverage (Figure 7; structures A and B, respectively). Importantly, in this T-p range the CO molecules adsorb only on the Co sites, in agreement with our recent study of adsorption of CO on pure Cu(111), where CO was found to adsorb only at step edges.[12]
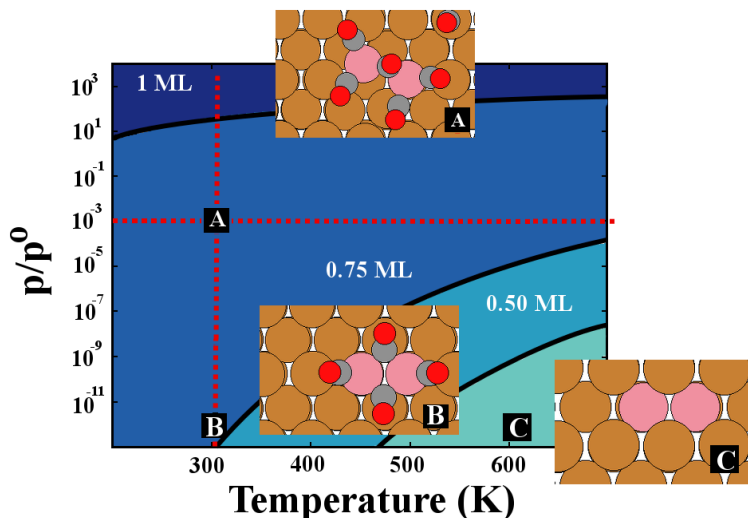
Fig. 7 T-p plot showing the CO/CuCo phase diagram in a wide range of T-p conditions. The solid black lines indicate the stability range of CO/CuCo phases, for three different CO coverages, in ML indicated in white. Some of the most stable CO/CuCo structures in ambient-pressure conditions are pictured in the insets.

5. CONCLUSION

Using STM, we followed the atomic structure of a CuCo alloy surface formed by evaporation of Co onto a Cu(110) single crystal. At low Co coverage (~0.2 ML) Co atoms substitute Cu atoms in the surface and subsurface forming small clusters of one or few Co atoms. Using XPS and IRRAS spectroscopies, together with DFT calculations, we determined the equilibrium structures formed by adsorption of CO on the bimetallic CuCo surface alloy. In the absence of CO, the Co atoms occupy preferentially second layer sites. In the presence of CO at pressures above 0.1 Torr CO pulls Co to the top surface layer and binds to it forming structures where multiple CO molecules attach to one Co atom. The multiple binding of CO molecules gives rise to shifts in the binding energy of the Co 2p core level peaks due to increased donation of electrons to CO, a

13

process akin to the formation of carbonyls. This means that the CuCo surface might have different catalytic properties than that of Cu or Co because such multiple CO adsorption on a single Co site weakens the M-CO bond and can thereby reduce the C-O bond scission probability. In addition to new fundamental information on the chemisorption of CO on alloy surfaces, this study might help explain the higher selectivity towards oxygenated products when CuCo is used instead of Co during the Fischer-Tropsch synthesis. Future design of bimetallic catalysts should take the peculiar behavior of the alloy constituents into account, and it is clear that further work on other bimetallic systems is necessary with the newly developed surface science techniques applicable in the presence of gases.

SUPPORTING INFORMATION

Reference APXPS and IRRAS spectra, HPSTM images at lower pressures, explanation of Gibbs free energy of the system, more details of our DFT calculations.

ACKNOWLEDGEMENTS

14

References

[1]Somorjai, G. A. *Introduction to Surface Chemistry and Catalysis*; Wiley-VCH: New York, **1999**.

[2]Ertl, G. *Angew. Chem. Int. Ed.* **2008**, *47*, 3524-3535.

[3]McIntyre, B. J.; Salmeron, M.; Somorjai, G. A. *Rev. Sci. Instrum.* **1993**, *64,* 687.

[4]Tao, F.; Tang D.; Salmeron M.; Somorjai G. A. *Rev. Sci. Instrum.* **2008**, *79,* 084101.

[5]Besenbacher, F.; Thostrup, P.; Salmeron, M. *MRS Bulletin* **2013,** *37,* 677.

[6]Hendriksen B. L. M.; Frenken, J. W. M. *Phys. Rev. Lett.* **2002**, *89*, 046101

[7]Ogletree, D. F.; Bluhm, H.; Lebedev, G.; Fadley, C. S.; Hussain, Z.; Salmeron, M. *Rev. Sci. Instrum.* **2002**, *73*, 3872.

[8]Salmeron, M.; Schlögl, R. *Surf. Sci. Rep.* **2008**, *63,* 169-199.

[9]Salmeron, M. *MRS Bulletin* **2013,** *38,* 650-667.

[10]Hoffmann, F. M. *Surf. Sci. Rep.* **1983**, *3*, 107-192.

[11]Zaera, F. *Chem. Soc. Rev.* **2014**, *43*, 7624-7663.

[12]Eren, B.; Zherebetskyy, D.; Patera, L, L., Wu, C. H.; Bluhm, H.; Africh, C..; Wang, L.-W.; Somorjai, G. A.; Salmeron, M. *Science* **2016**, *351*, 475-478.

[13]Eren, B.; Zherebetskyy, D.; Hao, Y.; Patera, L, L.; Wang, L.-W.; Somorjai, G. A.; Salmeron, M. *Surf. Sci.* **2016**, *651*, 210-214.

[14]Eren, B.; Liu, Z.; Stacchiola, D.; Somorjai, G. A.; Salmeron, M. *J. Phys. Chem. C* **2016**, *120*, 8227-8231.

[15]Alonso, D. M.; Wettstein, S. G.; Dumesic, J. A. *Chem. Soc. Rev.* **2012**, *41*, 8075-8089

[16]Nørskov, J. K.; Abild-Pedersen, F.; Studt, F.; Bligaard, T. *Proc. Natl. Acad. Sci.* **2011**, *108*, 937-943.

[17]Courty, P.; Durand, D.; Freund, E.; Sugier, A. *J. Mol. Catal.* **1982**, *17*, 241-254.

[18]Baker, J.E.; Burch, R.; Golunski, S.E. *Appl. Catal.* **1989**, *53*, 279-297.

[19]Subramanian, N.D.; Balaji, G.; Kumar, C.S.S.R.; Spivey, J. J. *Catal. Today* **2009**, *147*, 100-106.

[20]Xiang, Y.; Chitry, V.; Liddicoat, P.; Felfer, P.; Cairney, J.; Ringer, S.; Kruse, N. *J. Am. Chem. Soc.* **2013**, *135*, 7114-7117

[21]Prieto, G.; Beijer, S.; Smith, M.L; He, M.; Au, Y.; Wang, Z.; Bruce, D.A.; de Jong, K.P.; Spivey, J.J.; de Jongh, P.E. *Angew. Chem. In. Ed.* **2014**, *53*, 6397-6401.

[22]Mouaddib, N.; Perrichon, V.; Martin, G. A. *Appl. Catal. A* **1994**, *118*, 63– 72

[23]Buess, Ph.; Frans R.; Caers, I,; Frennet, A.; Ghenne, E.; Hubert, C.; Kruse, N. US 20030036573A1 Feb 2003.

[24]Iglesia, E. *Appl. Catal. A* **1997**, 161, 59–78.

[25]Lewis, E. A.; Jewell, A. D.; Kyriakou, G.; Sykes, E. C. H. *Phys. Chem. Chem. Phys.* **2012**, 14, 7215–7224.

[26]Lewis, E. A.; Le, D.; Jewell, A. D.; Murphy, C. J.; Rahman, T. S.; Sykes, E. C. H. *ACS Nano* **2013**, *7*, 4384-4392.

[27]Subramanian, N. D.; Balaji, G.; Kumar, C.S.S.R.; Spivey, J. J. *Catal. Today* **2009**, *147*, 100-106.

[28]Carenco, S.; Tuxen, A.; Chintapalli, M.; Pach, E.; Escudero, C.; Ewers, T. D.; Jiang, P.; Borondics, F.; Thornton, G.; Alivisatos, A. P.; Bluhm, H.; Guo, J.; Salmeron, M. *J. Phys. Chem. C* **2013**, *117*, 6259-6266.

[29]Hrbek, J.; Hoffmann, F. M.; Park, J. B.; Liu, P.; Stacchiola, D.; Hoo, Y. S.; Ma, S.; Nambu, A.; Rodriguez, J. A.; White, M. G. *J. Am. Chem. Soc.* **2008**, *130*, 17272−17273.

[30]Ling, W. L.; Takeuchi, O.; Ogletree, D. F.; Qiu, Z. Q.; Salmeron, M. *Surf. Sci.* **2000**, 450, 227–241.

[31]Mortensen, J.J.; Hansen, L.B.; Jacobsen, K.W. *Phys. Rev. B* **2005**, *71*, 035109.

[32]Blochl, P. E. *Phys. Rev. B* **1994**, *50*, 17953.

[33]Kresse, G.; Joubert, D. *Phys. Rev. B* **1999**, *59*, 1758.

[34]Perdew, J.P.; Chevary, J.A.; Vosko, S.H.; Jackson, K.A.; Pederson, M.R.; Singh, D.J.; Fiolhais, C. *Phys. Rev. B* **1992**, 46, 6671.

[35]Perdew, J.P.; Chevary, J.A.; Vosko, S.H.; Jackson, K.A.; Pederson, M.R.; Singh, D.J.; Fiolhais, C. *Phys. Rev. B* **1993**, 48, 4978.

[36]Falo, F.; Cano, I.; Salmeron, M. *Surf. Sci.* **1984**, *143*, 303-313.

[37]Biesinger, M C.; Payne, B. P.; Grosvenor, A. P.;. Lau, L. W. M; Gerson, A. R.; Smart, R. St. C. *Appl. Surf. Sci.* **2011**, *257*, 2717-2730.

[38]Eren, B.; Lichtenstein, L.; Wu, C. H.; Bluhm, H.; Somorjai, G. A.; Salmeron, M. *J. Phys. Chem. C* **2015,** *119*, 14669-14674.

[39]Tang, D.; Hwang, K.S; Salmeron, M.; Somorjai, G.A. *J. Phys. Chem. B* **2004**, *108*, 13300-13306.

[40]Yang, H.J.; Minato, T.; Kawai, M.; Kim, Y. *J. Phys. Chem. C* **2013**, *117*, 16429-16437.

[41]Toomes, R. L.; King, D. A. *Surf. Sci.* **1996**, *349*, 1-18.

[42]Xu, F.; Mudiyanselage, K.; Baber, A. E.; Soldemo, M.; Weissenrieder, J.; White, M. G.; Stacchiola, D. J. *J. Phys. Chem. C* **2014,** *118*, 15902-15909, and references therein.

[43]Tskipuri L.; Bartynski, R. A. *Surf. Sci.* **2009**, *603*, 802-806.

[44]Tremblay, B.; Manceron, L.; Gutsev, G.; Andrews, L.; Partridge, H. *J. Chem. Phys.* **2002**, *117*, 8479.

[45]Zhou, M.; Andrews, L. *J. Phys. Chem. A* **1998**, *102*, 10250.

[46]Frank, M.; Kühnemuth, R.; Bäumer, M.; Freund, H.-J. *Surf. Sci.* **2000**, *454-456*, 968.

[47]Mehl, S.; Ferstl, P.; Schuler, M.; Toghan, A.; Brummel, O.; Hammer, L.; Schneider, M. A.; Libuda, J. *Phys. Chem. Chem. Phys.* **2015**, *17*, 23538-23546.

[48]Baber, A. E.; Yang, X. F.; Kim, H. Y.; Mudiyanselage, K.; Soldemo, M.; Weissenrieder, J.; Senanayake, S. D.; Al-Mahboob, A.; Sadowski, J. T.; Evans, J.; Rodriguez, J. A.; Liu, P.; Hoffmann, F. M.; Chen, J. G. G.; Stacchiola, D. J. *Angew. Chem. Intern. Ed*. **2014**, *53*, 5336-5340.

[49]Wadayama, T., Kubo, K.; Yamashita, T.; Tanabe, R.; Hatta, A. *J. Phys. Chem. B* **2003**, *107*, 3768-3773.

[50]Reuter, K. *Catal. Lett*. **2016**, *146*, 541-563.

[51]Ruban, A. V.; Skriver, H. L.; J. K. Nørskov, J. K. *Phys. Rev. B* **1999**, *59*, 15990.

[52]Nilekar, A.U.; Ruban, A.V.; Mavrikakis, M. *Surf. Sci.* **2009**, *603*, 91-96.

[53]Collinge, G.; Kruse, N.; McEwen, J.-S. *J. Phys. Chem. C* **2017**, *121*, 2181–2191

Supporting Information

XPS Calibration of Surface Co Coverage

The Co coverage on the surface of the Cu(110) crystal was measured using the XPS peak intensities. Similar to deposition rate measurements with QCM, the Co surface layer underneath the oxygen top layer is calculated to have 21% Co and 79% Cu using the XPS Cu 2p and Co 2p peak intensities (85:15) and the Strohmeier equation [S1]. The 85:15 ratio remained unchanged throughout the experiments indicating Co neither desorbs via forming a carbonyl at pressures up to 0.5 Torr of CO nor it diffuses into the bulk.

CO Adsorption – Reference O 1s and C 1s Spectra

In this section, we compare the core level O 1s and C 1s spectra of CO adsorption on three surface: 1- our alloy CuCo surface, 2- a bare Cu(110) surface, and 3- a 10 ML Co thin film. The latter two are used as references for the pure Cu and Co metals.

Figure S1 shows an example of XPS spectra collected during CO adsorption on the surface, as well as reference measurements of CO adsorption on Cu(110) and on a thin Co film. On Cu(110), peaks arising from CO adsorption are at around 531.1 eV, and 286.1 eV with a strong satellite at 288.4 eV [27]. This strong satellite feature in the C 1s region is due to weak chemisorption of CO on Cu [S2]. On the 10 ML Co film, CO peaks appear at 531.7 and 285.7 eV without any satellite features. On the CuCo surface, the CO peaks appear at 531.9 eV and 285.7 eV, indicating that CO/CuCo has the same peak position as CO/Co in the O 1s region and peak position somewhere between CO/Co and CO/Cu in the C 1s region. However, in the C 1s region no satellite peak was observed for CO adsorbed on CuCo, which is an indicative of strong chemisorption (weaker than on pure Co but stronger than on pure Cu) [S2]. Both observations suggest that there are only few CO molecules are adsorbed on bare Cu(110), which occupies 79% of the surface.
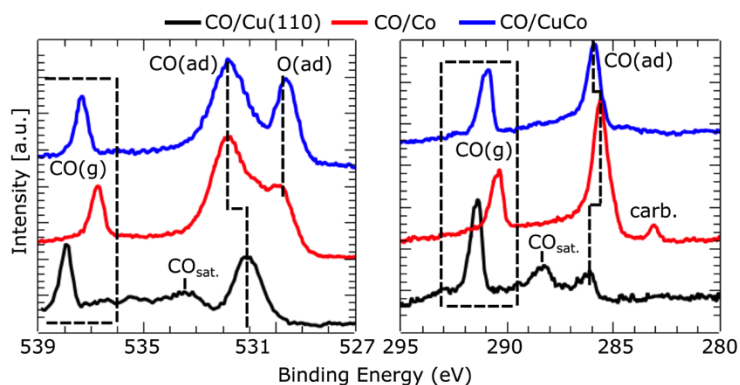
Figure S1 O 1s (left) and C 1s (right) regions of the XPS spectrum for CO adsorption on Cu(110) (black curve), on a Co 10 ML film (red curve), and on the CuCo alloy sample (blue curve). The black curve was acquired at 0.2 Torr, whereas the other two curves were acquired at 0.1 Torr CO. The boxed region indicate the gas phase CO(g) species, appearing at different energies due to different work function of the sample surface. The peak positions and line shapes of adsorbed CO(ad) species on the CuCo system is more similar to those on Co thin films than those on Cu(110).

CO Adsorption as a function of pressure

Figure S2 shows the O 1s and C 1s regions of the XPS spectra under various CO pressures. The peak positions and full width at half maximum (FWHM) in the O 1s and C 1s regions of CO adsorbed on CuCo remained unchanged in the pressure range of 1×10^{-6} to 0.5 Torr of CO (Figure S2).
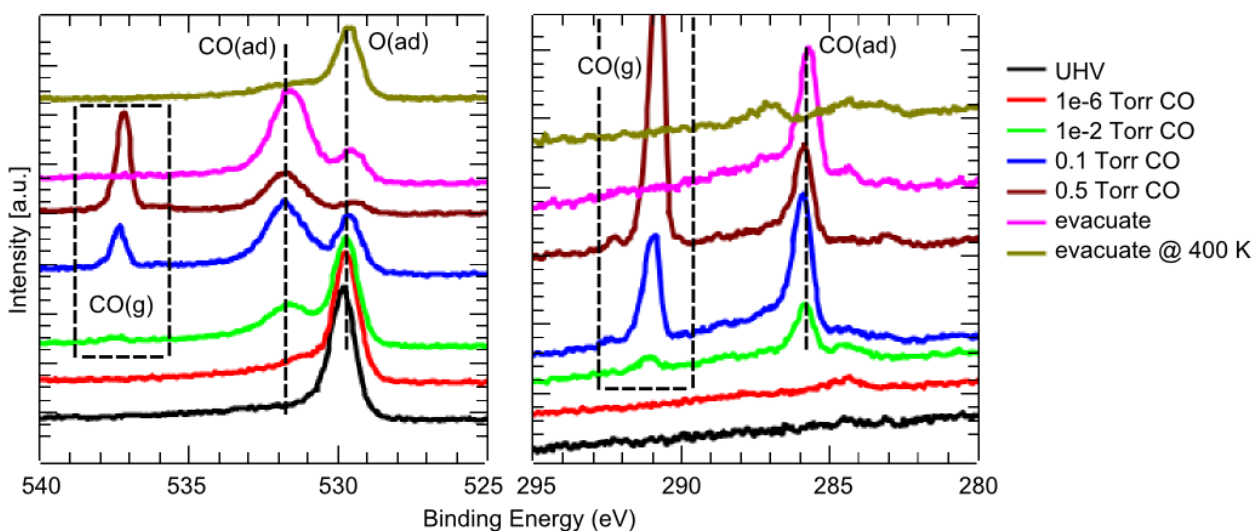

Figure S2 O 1s (left) and C 1s (right) regions of the XPS spectrum of the CuCo surface under various CO pressures. The surface is initially covered with atomic oxygen which produces the XPS peak at around 529.9 eV.

The CO adsorption peaks appear at approximately 531.9 eV and 285.7 eV, similar to those of CO adsorbed on a 10 ML Co thin film. The gas phase CO peak energies are above 537 eV and 291 eV (exact position depands on the work function), and they are shown inside dashed rectangular boxes. Once CO is removed from the gas phase and after the sample is heated up to 400 K, all the CO is removed from the surface. Small amounts of hydrocarbons desorbing from the chamber walls in the presence of CO in the Torr range, slowly contaminate the sample surface once CO is evacuated (peaks around 284.4 eV start to appear).The small peak around 283.2 eV is due to carbon in carbide-like species formed by contamination and beam damage effects. We minimized the increase of this peak by changing the measurement spot for each spectrum.

CO-induced Shifts in Co 2p

As explained in the main text, Co^0 $2p_{3/2}$ peak position from the CuCo alloy surface shifts to higher binding energies as the CO pressure is increased (Figure 3), when the Co surface population is around 20%. The same is true for the Co^0 $2p_{1/2}$, Co^{2+} $2p_{3/2}$, and the Co^{2+} $2p_{1/2}$ peak positions.

S2 – IRRAS

Because CO peak position depends on the adsorption site (e.g., Cu or Co, top-site or bridge-site, etc.), presence of atomic oxygen on the surface and CO coverage, we acquired various reference spectra at 90 K following a few Langmuir exposures and at RT under ambient CO pressure. The next three spectra are used as reference to interpret the IRRAS results shown in Figure 5 of the main text.
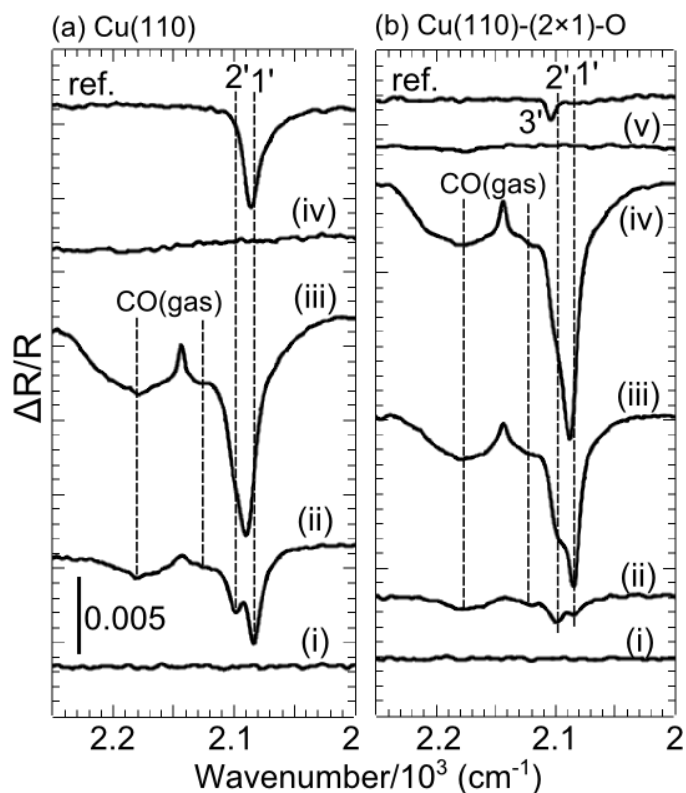
Figure S3 IRRAS spectra of CO at RT on: (a) bare Cu(110), and (b) oxygen-covered Cu(110)-(2×1)-O surfaces. In (a): (i) in UHV, (ii) in the presence of 0.02 Torr of CO, (iii) in the presence of 0.5 Torr of CO, (iv) after evacuation of CO. Top: reference spectrum after dosing 0.2 L of CO with the sample at 90 K. In (b): (i) in UHV, (ii) in the presence of 0.01 Torr of CO, (iii) in the presence of 0.1 Torr of CO, (iv) in the presence of 0.5 Torr of CO, (v) after evacuation of CO. Top: ref. spectrum after dosing 0.2 L of CO with the sample at 90 K. The peaks from adsorbed CO are marked with primed numbers: 1' at 2084-2086 cm^{-1} due to CO on Cu with coordination number (CN) =7; 2' at 2099 cm^{-1} from CO on Cu with CN=6; and 3' at 2104 cm^{-1} (in b-ref.) from CO on intact Cu(110)-(2×1)-O. The absence of this feature in other spectra in (b) is due to the negligible amount of adsorbed CO, due to its low adsorption energy on the oxygen-covered surface. In this surface CO adsorbs only on vacant Cu sites created by the CO+½O→CO$_2$ reaction. The scale bar is the same for (a) and (b). The reason behind the emergence of peak 2' is explained in Ref. [14]. Reprinted with permission from Ref. [14]. Copyright (2016) American Chemical Society.
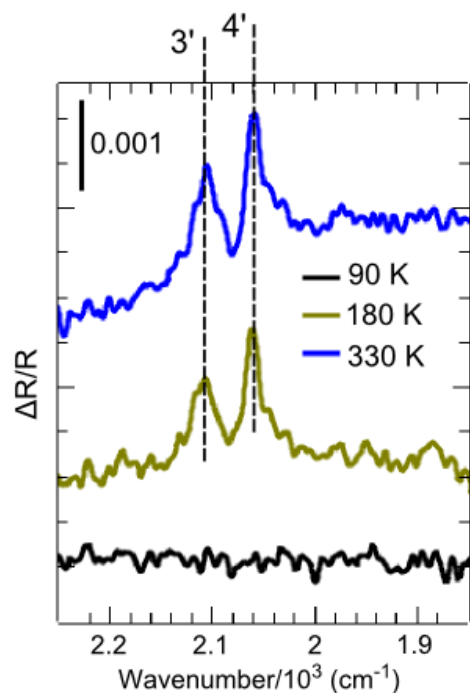
Figure S4 IRRAS spectra of CO desorption from the oxygenated CuCo surface. As discussed in the previous figure, peak 3' at 2105 cm^{-1} originates from CO on intact Cu(110)-(2×1)-O, while peak 4' at 2057 cm^{-1} is due to CO desorbed from an under-coordinated top Co site with a co-adsorbed oxygen. The surface Co population was around 0.1 ML in this case.
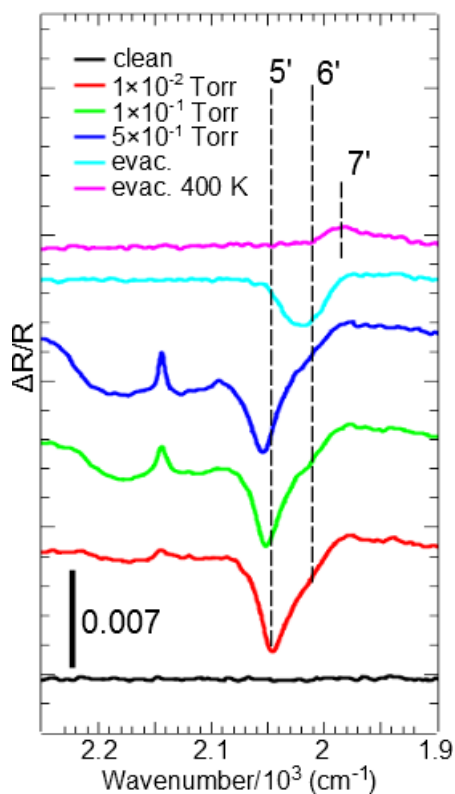
Figure S5 IRRAS spectra of from CO adsorption at RT on a 10 ML Co film (no Cu is present on the top surface). As discussed in [33], CO adsorbs first on bridge sites at low coverage, and later on top sites at high coverage on the Co films.

Table S1 Approximate stretching frequencies for different CO adsorption sites on the CuCo surface. Since the surface is in equilibrium with gas phase CO. The CO coverage is high, especially on the Co sites.

Adsorption site	Wavenumber (cm^{-1})	SI name	On the main text
Copper CN=7, top site	2084-2086	1'	1'
Copper CN=6, top site	2099	2'	-
Copper CN=6, top site, co-adsorbed oxygen	2104	3'	-
Cobalt, CN=6, top site, co-adsorbed oxygen	2057	4'	-
Cobalt, under-coordinated, top site, compressed	2048-2055	5'	2'
Cobalt, top site	2015-2020	6'	3'
Cobalt, CN=7, bridge site	1980-1983	7'	5' (becomes 4' at high coverage)
Co^{2+} residuals	2184	-	6'

S3- HPSTM

Bare Cu(110)

We start with discussing the structural changes on a bare Cu(110) surface in the presence of 1 Torr of CO at RT, which was discussed in detailed in our previous work [14]. We have reported that this surface breaks up into clusters a few nanometer long oriented along the [1-10] direction and separated by typically two atomic distances, i.e., 0.72 nm in the [100] direction with (1×2) periodicity. This restructuring of the Cu(110) surface in the presence of CO is different than that of the model CuCo(110) surface used in the present work (Figure 4).

CuCo before Reduction

As shown in our previous work, p(2×1)-O reconstruction on Cu(110) remains for long times at CO pressures below 0.02 Torr at 298 K [32] due to high binding energy of atomic oxygen in the added rows (around 2 eV) [S3]. This is also partially the case for the CuCo surface. Examples are shown in the low and high magnification HPSTM images in Figure S6a and b, respectively. It is not clear from these images if the clusters on the surface are pure Co (i.e., phase separation), or they are the initial nano-islands formed during the sample preparation process. However, there is a considerable amount of adsorbed CO (0.13 ML) already at 0.01 Torr on this surface compared to Cu(110)-p(2×1)-O which was below 0.01 ML (coverages estimated from APXPS measurements) [14, 32]. CO probably adsorbs on Co rich parts and breaks the (2×1) periodicity. The surface does not exhibit this periodicity in Figure S6b are Co, although CO may have not entirely removed the initial oxygen attached to it. In summary, the surface is a mixture of ordered O on Cu(110) and disordered O+CO on Co in this pressure range.
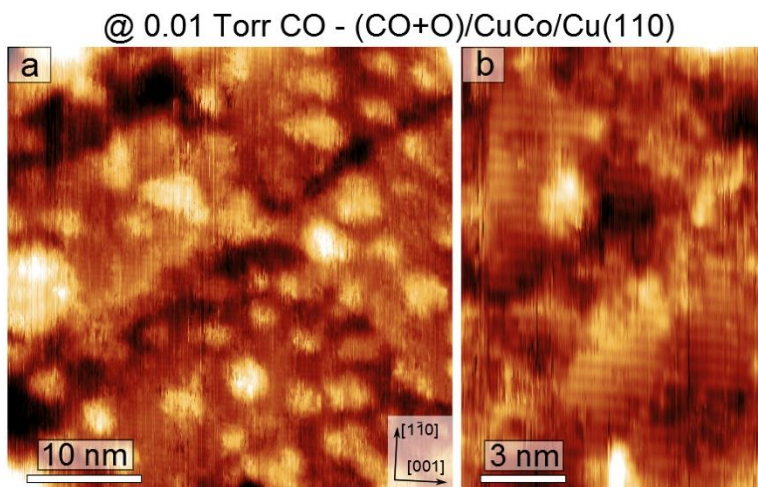

@ 0.01 Torr CO - (CO+O)/CuCo/Cu(110)

Figure S6 STM image at 0.01 Torr of CO. (2x1)-O structure is mostly intact at pressures below 0.1 Tor of CO, although in some other areas it starts to disappear and form irregular clusters. We attribute these to Co-rich sites, on which CO can adsorb.

CuCo after Reduction

At 0.1 Torr and above, the p(2×1)-O structure is removed completely by reaction with CO (O + CO → CO_2) After this up to 0.5 ML of CO adsorbs on the CuCo surface. Between 0.5 and 3 Torr of CO, the surface is broken up into linear clusters oriented along the [001] direction (Figure S7a).
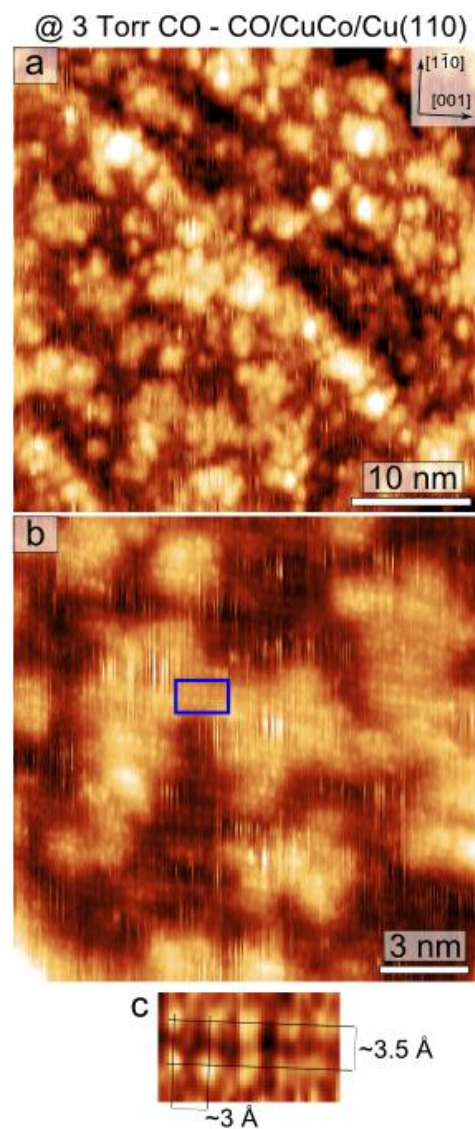
In addition to the discussion in the main text, figures S7b and S7c we found that atomic resolution could be only observed on the linear structures visible in Figure S7b. Streaky traces on the other parts of the surface is due to high adsorbate mobility, likely due to CO weakly adsorbed on Cu sites. The weakening of the adsorption is due to steric repulsion between CO molecules, which also blocks CO adsorption at Cu sites next to the Co atoms very unlikely. However CO can adsorb on Cu sites far away from Co sites, but unlike on the bare Cu(110) surface [14], no (1×2) reconstruction is observed in the alloy surface.

@ 3 Torr CO - CO/CuCo/Cu(110)

a

[1 1̄0]
[001]

10 nm

b

3 nm

c
~3.5 Å
~3 Å

Figure S7 After the O-layer is removed by reaction with CO at a pressure of 0.5 Torr and higher, CO adsorbs on the CuCo(110) surface and forms a peculiar adlayer structure in certain areas which are probably Co-rich. Cu and Co cannot be distinguished from their STM contrast in these images. No (1×2) structure related to CO/Cu(110) can be observed.

S4- DFT

Gibbs Free Energy Formalism

We use surface Gibbs free energies—a formalism extensively employed to study materials under working conditions [S4-S5]—to compare the stability of different CO/CuCo phases, with the following formulation: the Gibbs free energy $\Delta G(\theta,\chi)$ of the CO/CuCo system depends on the CO coverage, θ, defined as the number of CO molecules per area unit, and the Co surface percent population, χ, defined as the number of Co atoms at the surface with respect to the total number of Co atoms in the cell. We computed surface Gibbs free energies $\Delta G(\theta,\chi)$ according to Eq. 1

$$\Delta G(\theta, \chi) = (E_{CO\text{-}CuCo} - N_{Cu}E^{Bulk}_{Cu} - N_{Co}E^{Bulk}_{Co} - N_{CO}E_{CO} - N_{CO}T\Delta S_{ads} - N_{CO}k_b T Ln(p/p^0))/A \quad (1)$$

where $E_{CO\text{-}CuCo}$, E^{Bulk}_{Cu} and E^{Bulk}_{Cu} are respectively the total energy of the alloy—for a given χ solute distribution—and the total energy of bulk Cu and Co. E_{CO}, on the other hand is the total energy of gas CO. N_{Cu}, N_{Co} and N_{CO} are the number of Cu and Co atoms in the unit cell, and the number of CO molecules in the CO/CuCo system. T is the temperature and p is the CO pressure with respect to the standard pressure p^0 equal to 1 atm. k_b is the Boltzmann constant and A is the area of the unit cell (73.72 Å^2). We referred the ΔG values with respect to the surface energy value for the most stable solute arrangement (93 meV/Å^2). ΔS_{ads} is the entropy change for the adsorption defined as in

$$\Delta S_{ads} = (S_{CO\text{-}CuCo} - N_{Cu}S^{Bulk}_{Cu} - N_{Co}S^{Bulk}_{Co} - N_{CO}S^0_{CO}) \quad (2)$$

we assume $S_{CO\text{-}CuCo} \sim N_{CO}S^{Ads}_{CO} + S_{CuCo}$ and neglect the formation entropy of the alloy in comparison to the gas adsorbate so that ΔS_{ads} becomes

$$\Delta S_{ads} = N_{CO}(S^{Ads}_{CO} - S^0_{CO}). \quad (3)$$

In Eq. 3 S^0_{CO} is the standard entropy of gas CO (195 J/molK at 273K in agreement with NIST [S6]) and S^{Ads}_{CO} is the entropy of adsorbed CO. We used the empirical relationship developed by Campbell [S7] to describe the entropy of adsorbed adsorbates: $S^{Ads}_{CO} \sim 0.7 \, S^0_{CO}$.

In order to construct ΔG maps (Figure 6) we studied CO-CuCo structures with increasing Co surface population χ, from zero for the case in which all Co is located in the subsurface to 100% when both Co atoms in the unit cell populate the Cu matrix surface. At each χ value we addressed the adsorption of CO for a range of increasing coverage, from zero to 1ML. For each coverage, we found the most stable adsorption arrangement for CO in the CuCo cell, considering

27

all possible Cu and Co adsorption sites. That gave a grid of (7x3) ΔG values. A continues ΔG map was created by interpolating the Gibbs free energy values in the grid. We report average binding energies E_b in Table S2 for all structures in the ΔG grid and the atomistic structures of the CO-CuCo phases are displayed in Figure S8. E_b were all computed with respect to the most stable CuCo arrangement in the absence of CO as in

$$E_b = (E_{CO\text{-}CuCo} - E_{CuCo} - N_{CO}E_{CO})/N_{CO} \tag{4}$$

Table S2. Calculated CO average binding energies E_b in eV for three different Co surface populations χ—0% with Co atoms located in the subsurface of the Cu(110) matrix and 100% with Co located in the surface of the Cu(110) matrix, and 50% with Co located on the surface and subsurface—and increasing CO coverage in ML. Binding energies were referred to the most stable CuCo substrate in the absence of CO.

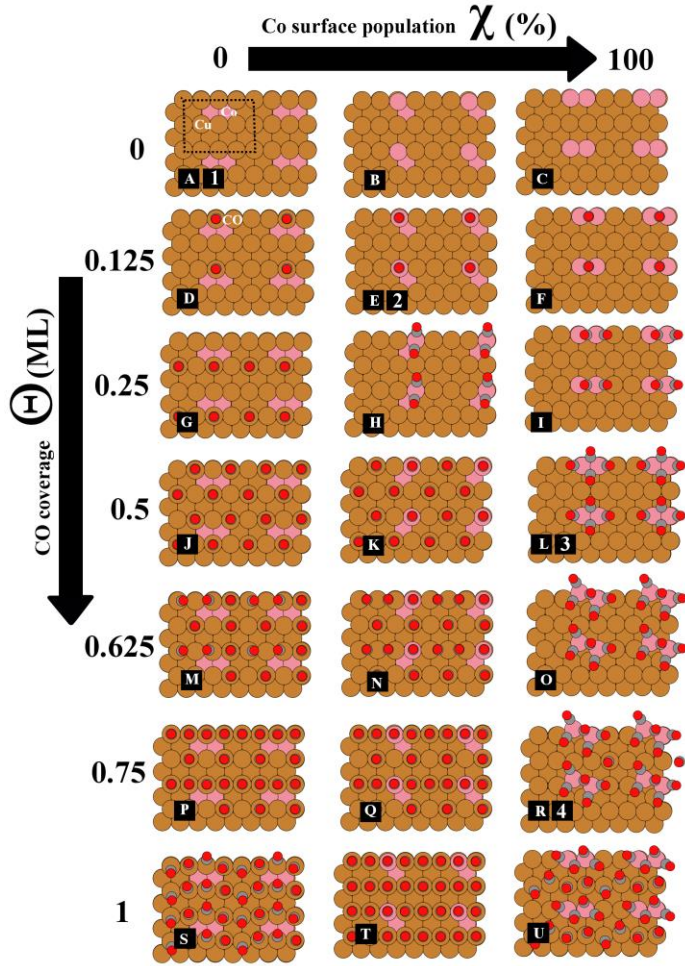|	CO Coverage (ML)						
χ	0	0.125	0.25	0.5	0.625	0.75	1
0%	--	–0.71	–0.75	–0.84	–0.82	–0.60	–0.58
50%	--	–1.50	–1.37	–1.05	–1.01	–0.73	–0.57
100%	--	–1.11	–1.48	–1.50	–1.30	–1.25	–0.96

Figure S8 Atomistic structures of the different CO/CuCo phases used to build Fig 6 including the bare p(4x2) unit cell (Top Left structure). The structures were depicted as 2x2 replicated unit cell for clearness. The numerical labels refer to the structures presented in the main text.

Surface Structure of CO/CuCo

In the absence of CO, Cobalt atoms are located in the subsurface of the Cu(110) matrix forming Co dimers (d_{Co-Co}=2.37Å). The energy to separate these dimers from its most stable arrangement until d_{Co-Co}=5.11 Å is 119meV/Co. We further computed segregation energies, E_{Seg}, defined per Co atoms as in

$$E_{Seg}= (E_{CuCo}(\chi=100\%)–E_{CuCo}(\chi=0\%))/N_{Co}, \tag{5}$$

where $E_{CuCo}(\chi)$ is the total energy of the CuCo substrate for a give Co surface population. E_{Seg} is the energy needed to move the metal impurity from the bulk of the host material to the surface: the lower is E_{Seg} the stronger would be the tendency for the Co impurity to segregate to the surface. E_{Seg} in the absence of CO was 348 meV, being this value positive and in qualitative agreement with the literature [42, S8]. This means that in the absence of CO segregation of Co is

29

thermodynamically unfavorable and will not happen under normal conditions. This also means that in the absence of CO the surface will mostly contain Cu while the Co atoms will be located in the subsurface. However, this does not necessarily may be observed experimentally because at RT might the Co adatoms diffuse too slowly into the subsurface. Also surface oxygen reduces the surface energy. E_{Seg} was found to be –234 meV at 1 ML CO coverage. The fact that this value is negative indicates that in the presence of CO Co prefers to segregate and hence the surface would mostly contain the Co component of the alloy. Similar effect has been found for other adsorbates and substrates [S9].

We now address the energetics of CO adsorption in the CuCo substrate for increasing CO coverage. The calculated CO average binding energy E_b for different Co surface populations are reported in Table S2. Our results indicate that CO molecules adsorb on the different Cu top sites of the surface when Co populates the subsurface of the Cu matrix. A moderate binding energy increase with coverage was found, suggesting weak CO-CO repulsion. Differently, CO molecules bond to the Co top sites with a more pronounced CO-CO repulsion (See Figure S8 for more detail on the structures). These observations are consistent with the stronger affinity of CO to Co compared to Cu.

In order to bring more insight into the distribution of CO molecules in the CuCo substrate, we display in Figure S9 (Right Panel) a plot of the number of CO molecules adsorbed per Co atom for increasing CO coverage. The results indicate that Co sites are able to accommodate several CO molecules, with a maximum of 2.5 CO molecules/Co site for CO coverage of 0.6-0.8ML.
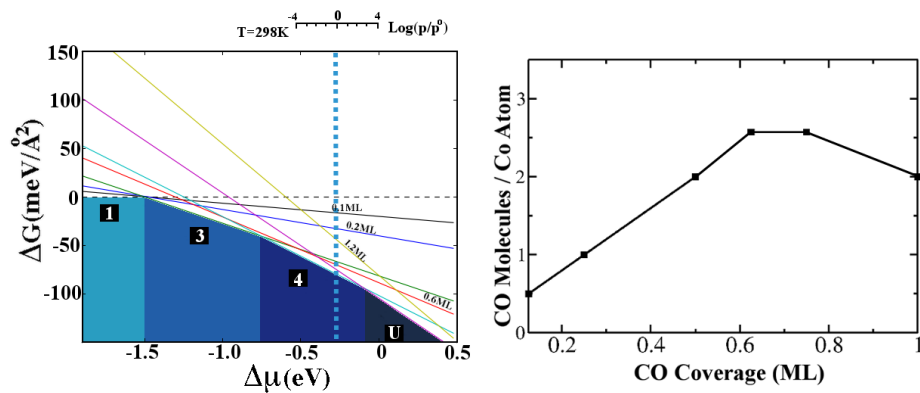
Figure S9 (Left panel) Gibbs free energies ΔG as a function of the chemical potential of CO. The additional axis on the top gives the corresponding pressure scales at T=298K. The lighter area represents the clean CuCo alloy surface without CO. The blue dashed lines highlights the working ambient-pressure conditions. See Figure S8 for the structure labels. (Right panel) Number of CO molecules per Co atom, for increasing CO coverage.

We finally address the structure of CO/CuCo in the presence of CO at ambient temperature and pressure conditions. Figure S9 (Left Panel) shows a free surface energy plot ΔG ($\Delta\mu$) as a function of the CO chemical potential of $\Delta\mu$,

$$\Delta G(\Delta\mu) = (E_{CO\text{-}CuCo} - N_{Cu}E^{Bulk}_{Cu} - N_{Co}E^{Bulk}_{Co} - \Delta\mu)/A \qquad (6)$$

Figure S9 include all CO/CuCo structures at increasing CO coverage at different Co surface populations. This is contrast to Figure 7 in which only the most stable CO-CuCo phases are visible. For low CO chemical potential, the most stable phase is the bare CuCo substrate with Co atoms populating the subsurface. The adsorption of CO only starts once $\Delta\mu$ reaches the critical value of 1.5 eV. At moderate and high $\Delta\mu$ values, CO molecules adsorb on the Co sites leading to 0.5ML and 0.75 ML. Our results indicate that CO/CuCo phases with 0.75 ML CO coverage are present in the phase diagram at ambient conditions, containing of five CO molecules bonded to the Co sites and a single CO molecule bonded to Cu. The average C-O distance in the 5CO-Co moiety is 1.18 Å (molecules 1-5 in Figure S10 Top panel), being this distance 1.14 Å for the CO molecule bonded to Cu (molecule 6 in Figure S10 Top panel). Both distances are slightly larger than for the case of gas CO (1.13 Å). The average C-Co distance is 1.79 Å for the top CO molecules in the 5CO-Co moiety (molecules 1, 2, 3 and 5 in Figure S10 Top panel), being 1.93 Å for the bridge CO (molecule 4 in Figure S10 Top panel). The C-Co distance for the CO bonded to Cu is 1.86 Å (molecule 6 in Figure S10 Top panel). We found in the experiments that the adsorption of CO pulls the Co atoms away from the surface. The average vertical distance of the Co atoms with respect to the outermost CuCo(110) plane is 0.51 Å.
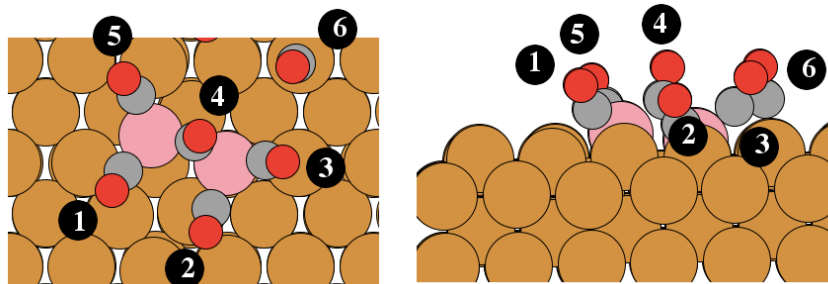

Figure S10 Top and side views of the most stable CO/CuCo phase at working conditions (structure 4 on Figure 6 and R on Figure S8). Each CO molecule in the CO-CuCo moiety has been numbered.

Computational parameters

We finally provide convergence tests with respect to the *k*-points, the grid spacing parameter *h* and the smearing of the occupation numbers. The results reported in Table S3 indicate that our binding energies are converged within 0.02 eV and the surface Gibbs free energy within 1meV/Å^2.

Table S3. Binding energies with three significant figures for most stable CO/CuCo phase at working conditions (structure R on Figure S8) with respect to the *k*-point sampling, the grid spacing parameter *h*, and the smearing of the occupation numbers.

	k-point grid				
	(2x2x1)	(2x4x1)	(2x6x1)	(3x4x1)	(4x6x1)
E_b, eV	−1.250	−1.278	−1.268	−1.248	−1.254
	h				
	0.18	0.17	0.15	0.12	0.1
E_b, eV	− 1.250	− 1.229	− 1.265	− 1.268	− 1.273
	Fermi Energy, eV				
	0.1		0.05		0.01
E_b, eV	−1.250		−1.254		−1.256

In order to estimate the impact of the exchange-correlation functional and the inclusion of van der Waals corrections, we carried DF calculations with RPBE [S10] and vdW-DF2 [S11] for a set of selected structures. Binding energies are reported in Table S4 and Gibbs free energy diagrams with respect to the chemical potential of CO are displayed in Figure S11. The results indicate the well-known overbidding of PW91 in comparison to RPBE, which in general reports more positive binding energies [S12]. The vdW-corrected binding energies lay in between the PW91 and RPBE values. The phase diagrams for RPBE and vdW-DF2 in general are shifted towards more positive CO chemical potentials, and the crossing points between different CO-CuCo phases is functional dependent, as these depend on the binding energies. Still, under working conditions, structure 4 remains the most stable CO-CuCo phase.

Table S4. Binding energies for some of the most stable CO/CuCo phases (structures E, L, R and U on Figure S8) for different exchange-correlation functional.

E_b, eV	0.125ML	0.5ML	0.75ML	1ML
PW91	–1.50	–1.50	–1.25	–0.96
RPBE	–0.89	–1.08	–0.88	–0.58
vdW-DF2	–1.21	–1.05	–0.93	–0.67

References

[S1] Strohmeier B. R. *Surf. Interface Anal.* **1990**, *15*, 51-56.

[S2] Hüfner, S. *Photoelectron Spectroscopy - Principles and Applications*; Springer-Verlag: Berlin Heidelberg, 2003.

[S3] Duan, X.; Warschkow, O.; Soon, A.; Delley, B.; Stampfl, C. *Phys. Rev. B* **2010**, 81, 075430.

[S4] Reuter, K; Scheffler, M. *Physical Review B* **2001**, 65, 035406.

[S5] de Smit, E.; Cinquini, F.; Beale, A.M.; Safonova, O.V.; van Beek, W.; Sautet, P.; Weckhuysen, B.M. *J. Am. Chem. Soc*. **2010**, 132, 14928-14941.

[S6] www.nist.gov

[S7] Campbell, C. T.; Sellers J. RV. *J. Am. Chem. Soc*. **2012,** 134**,** 18109-18115.

[S8] Nilekar, A. U.; Ruban, A. V.; Mavrikakis, M. *Surf. Sci.* **2009**, 603, 91-96.

[S9] Menning, C. A.; Chen J. G. *J. Chem. Phys.* **2009**, 130, 174709.

[S10] Hammer, B; Hansen, L. B.; Nørskov J. K., *Phys. Rev. B* **1999**, 59, 7413.

[S11] Lee, K.; Murray, D. E.; Kong, L.; Lundqvist, B. I.; Langreth, D. C. *Phys. Rev. B*, **2010**, 82, 081101.

[S12] Wellendorff, J.; Silbaugh, T. L.; Garcia-Pintos, D. ; Nørskov, J. K.; Bligaard, T.; Studt, F.; Campbell, C. T. Surf. Sci. **2015**, 640, 36-44.